Environment Canada
Environnement Canada

Deformation and Flow of Barnes Ice Cap, Baffin Island

G. Holdsworth

SCIENTIFIC SERIES NO. 52
(Résumé en français)

INLAND WATERS DIRECTORATE,
WATER RESOURCES BRANCH,
OTTAWA, CANADA, 1975.

ERRATA

Page 9

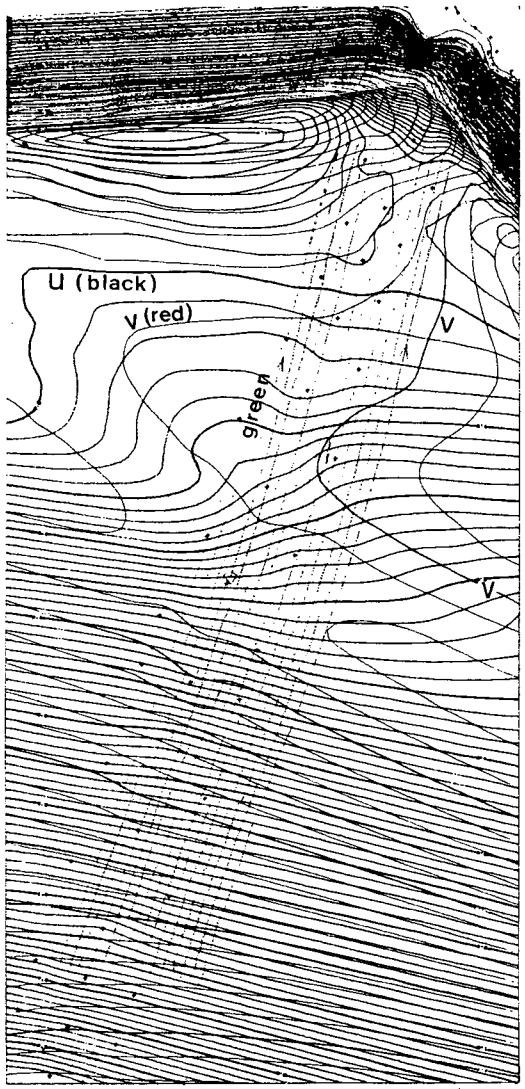

Figure 8. (a) Plot of velocity components u,v, and flow lines generated from them.

Page 15

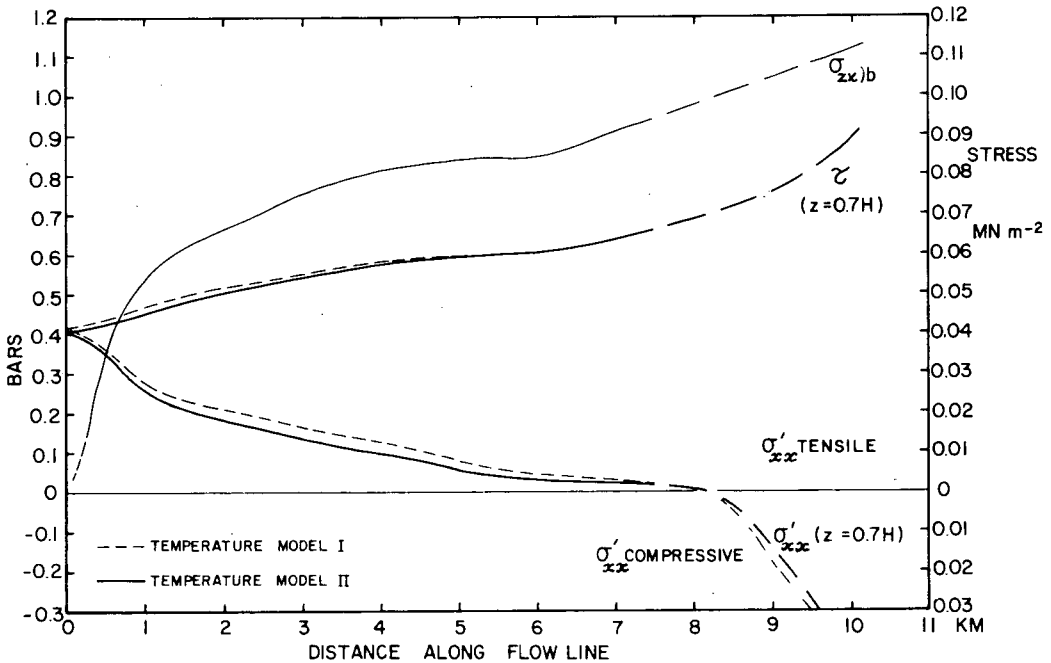

Figure 14. Variation of stresses at the base and at about $0.3H$ above the base along the flow line ON. Beyond $x = 7.5$ km variation is only approximate as $|\sigma'_{yy}|$ increases to become comparable to $|\sigma'_{xx}|$.

Page 15

Section (a), line 6: $R = n + 1/n + 2$ should read $R = (n + 1)/(n + 2)$.

ADDENDUM

Page 7

Para. 2, line 2: The General Purpose Contouring Program is supplied by California Computer Products Inc.

Environment Canada
Environnement Canada

Deformation and Flow of Barnes Ice Cap, Baffin Island

G. Holdsworth

SCIENTIFIC SERIES NO. 52
(Résumé en français)

INLAND WATERS DIRECTORATE,
WATER RESOURCES BRANCH,
OTTAWA, CANADA, 1975.

Cat. No.: En 36-502/52

CONTRACT # KL327-4-8069
THORN PRESS LIMITED

Contents

Tables

Tables (cont.)

Illustrations

Illustrations (cont.)

Abstract

Measurements taken in 1970 and 1971 of the positions of 43 surface stations along a transect (10.4 km long) from the divide to the northeast margin of the south dome of Barnes Ice Cap, have enabled surface velocities and strain rates to be computed along surface "flow lines" generated from the velocity distribution. Using a variation of a method developed by Budd (1969), the parameters $n = 4.2 \pm 0.1$ and $B = 11.9$ (± 1.0). MN $m^{-2}s^{1/4.2}$ in the flow law are determined for the stress range $0.05 < \tau < 0.1$ MN m^{-2} where τ is the effective stress. From the measured vertical velocities of the ice and the buildup of superimposed ice over the period 1970-73, it appears that this part of the ice-cap surface is rising. This is not necessarily the case elsewhere or when averaging is done over longer periods of time. More data are required before it is known whether the divide is stable or is still migrating, as the result of a surge.

Résumé

Les mesures effectuées en 1970 et 1971 sur la position de 43 stations d'observation en surface le long d'une virée transversale de 10.4 km, entre la ligne de partage et la marge nord-est du dôme sud de la calotte glaciaire Barnes, ont rendu possible le calcul des vélocités superficielles et des taux de déformation le long des lignes de flux déterminées par la distribution cinétique. À l'aide d'une variante d'une méthode créée par Budd (1969), les paramètres $n = 4.2 \pm 0.1$ et $B = 11.9$ ($\pm$ 1.0). MN $m^{-2}s^{1/4.2}$ dans la loi du flux sont déterminés en fonction de l'échelle de contrainte $0.05 < \tau < 0.1$ MN m^{-2}, où τ représente la contrainte effective. Il ressort des vélocités verticales mesurées de la glace et de l'accumulation de la glace entre 1970 et 1973 que cette partie de la surface de la calotte glaciaire s'élève. Cela n'est pas nécessairement le cas ailleurs ou lorsque la moyenne est établie en fonction de périodes plus longues. Il faut recueillir plus de données avant de pouvoir déterminer si la ligne de partage est stable ou encore en déplacement par suite d'une crue.

Deformation and Flow of Barnes Ice Cap, Baffin Island

G. Holdsworth

INTRODUCTION

The present program was initiated to study the dynamics of the south dome area of Barnes Ice Cap (69° 45' N; 172° 15' W) which possesses some characteristics that are not well understood in general. One of these is the thermal regime which has feedback into the dynamic behaviour of the ice cap. Owing to the formation of superimposed ice, the ice temperature at the top (20 m below the surface) of the south dome area is about 8° higher than the mean annual air temperature and 3.5° higher than the marginal ice temperature. Such a condition may have persisted for a long period of time; in which case there is a strong possibility that the basal ice temperature beneath the divide may be at or close to the pressure melting temperature.

Another phenomenon is the occurrence, on certain areas of the ice cap including one on the south side of the south dome, of highly irregular surface topography that is almost certainly due to surges (Løken, 1969; Holdsworth, 1973a). Surges may be intimately linked with the thermal regime and imply that at least part of the base of the ice has been at the pressure melting temperature. The occurrence of narrow transverse crevasses, spaced about 50 m apart and extending down the ice cap to at least 3.5 km from the divide, may be related to the foregoing phenomenon. The crevasses are still sustained under a longitudinal stretch of 1.6×10^{-3} a^{-1} across the divide.

The divide, defining the southwest end of the present survey, has been displaced to the northeast by a relatively recent surge (Holdsworth, 1973a). The ice-cap profile lying to the southwest of the divide has not yet recovered from the surge; one of the purposes of this paper is to present data that might show whether the northeast profile has fully adjusted to the new divide and whether the latter is stable.

Løken, Geiger and Langlais (1968) give preliminary measurements of ice movement at three poles near the northeast margin of the south dome, where movements of nearly 5 m yr^{-1} were determined at about 1.5 km from the ice edge. Stations A and B on bedrock outcrops were used for the survey and had been assigned geographic co-ordinates earlier, as a result of geodetic measurements by Henderson in 1966.

The present survey, based on observations made in 1970 and 1971, uses these two stations, as they form a conveniently oriented base line from which movement vectors for stations on the ice may be determined. The positions of these stations have been used to provide horizontal and vertical control for ice depth values determined in 1970 (Jones, 1972).

INSTRUMENTS

For the 1970 and 1971 surveys the following instruments and accessories were used:

- two Wild T2 theodolites, one of which was adapted for accepting the aiming head of the Distomat,
- one Wild DI-10 Distomat (serial number 10510),
- three prism reflectors,
- four Wild targets,
- seven tripods,
- two MRA-3 Tellurometers, and
- two Wallace and Tiernan (0-7000 ft) altimeters with thermometers and hygrometers.

METHOD OF SETTING OUT THE NETWORK

The centre line of the network was laid out as near as possible along a flow line, which was assumed to be running down the line of maximum slope. The centre line consists of two straight segments deviating by 3.5° from one another at 4.5 km from the divide. Using the Distomat, the network of poles was set out from May 23 to May 29, 1970. The array (Fig. 1) was designed as a series of linked

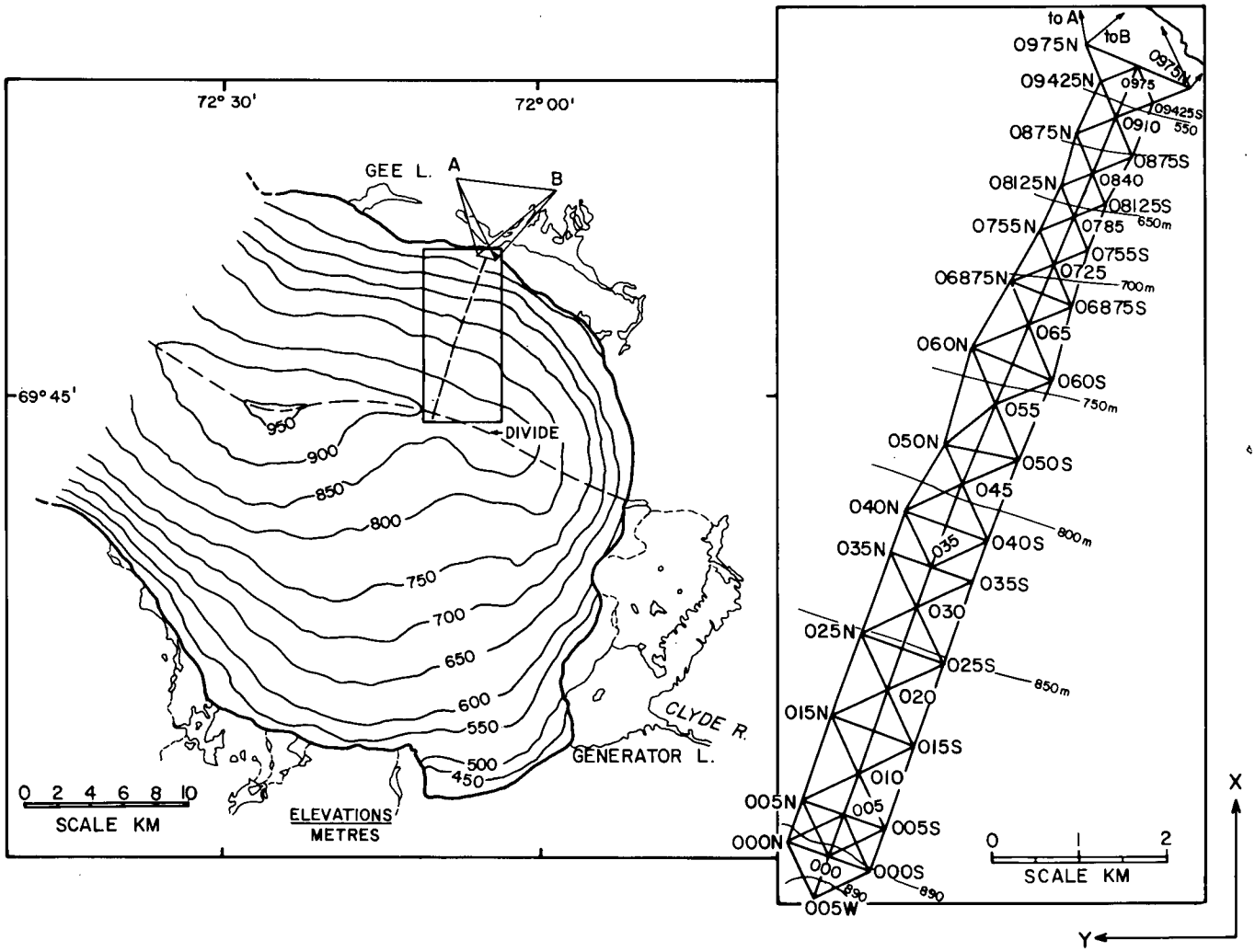

Figure 1. Map of south dome of Barnes Ice Cap showing location and structure of the array of reference points in the ice.

diamonds of diagonal distance $\leqslant 1$ km. This latter distance was dictated by the range of the Distomat rather than by the curvature of the ice cap down to about 4.5 km from the divide. Beyond this point the curvature of the ice cap forced a progressive reduction in the size of the diamonds.

The whole ice-cap network could be covered by using only the Distomat—a relatively simple instrument with which distances may be rapidly measured. The network was stopped about 0.5 ± 0.1 km from the edge of the ice cap on account of increasing debris within the ice (which hindered drilling operations), increasing curvature of the surface, and because the ice depths were too shallow beyond here to get results using a 35 MHz radio echo sounder (Jones, 1972). The deformation of the marginal areas is complicated by the existence of structures within the ice (Hooke, 1973a, b).

The poles were aluminum tubing, 1.25 in. (3.175 cm) o.d. and 16 ft (4.88 m) long, originally set in the ice so that approximately 4 m was frozen-in. This was accomplished by pouring water onto the ice chips and filling the remainder of the hole. The reference point for the stations was the top centre of the pole. A 1-foot (0.3-metre) sleeve with hose clamps enabled an extension pole, 2.44 m long, to be attached for identification purposes. This was removed for surveying purposes. In 1971 it was still possible to set up over each pole without having to cut the tube or use an eccentric station.

SURFACE MASS BALANCE MEASUREMENTS, 1970-73

In the spring months (May, June) of the 1970-73 period, soundings were taken at each station to determine the net gain or loss of ice, as well as firn and snow depths (Table 1). Figure 2 shows surface superimposed ice gain or loss versus elevation over the period from fall 1969 to fall

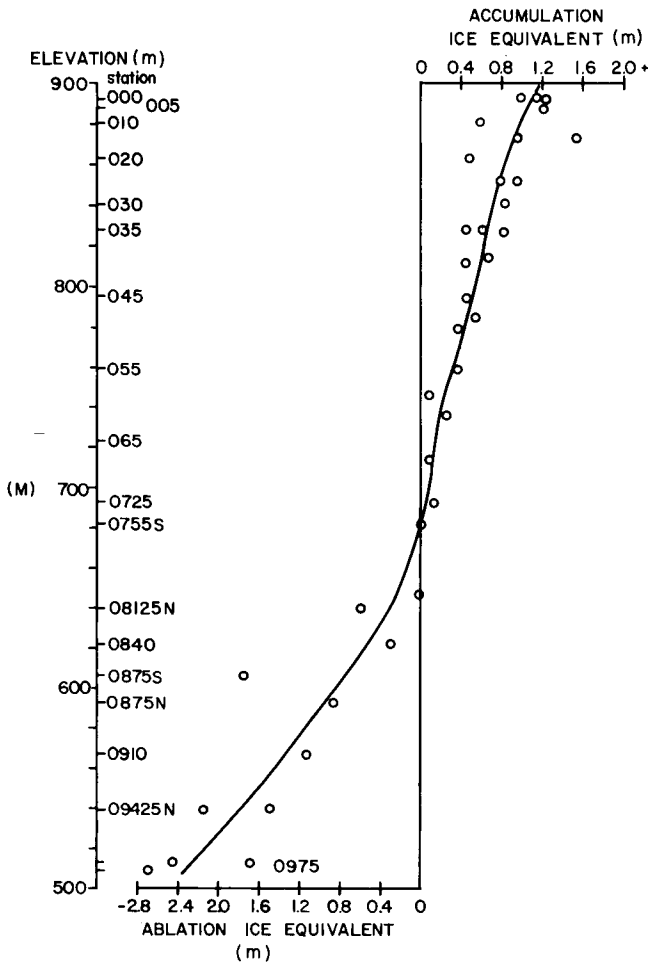

Figure 2. Net ice balance over the period from fall 1969 to fall 1972.

1972. The net carry-over of old snow or firn into the spring 1973 is not included, as the prime concern is to obtain an *average* value of ice gain or loss over a period of several years. This can then be compared with the vertical ice flow rates.

Table 1. Snow and Firn Thickness

Year	Mean snow depth (cm)	Standard deviation (cm)	Number of poles	Extent of firn location/average thickness (cm)
1970	108.1	26.1	42	not available
1971	133.6	23.5	43	divide /48 to pole 06875S /0
1972	115.1	19.5	43	divide /32 to pole 035S /0 (uncertain)
1973	121.5	8.5	40	divide /30 to pole 0725 /0

Note: average snow density = 350 kg m^{-3}
firn density = 500 kg m^{-3}

SURVEY PROCEDURE

The 1970 survey lasted 28 days (May 31 to June 27); 12 days were lost due to the weather. In 1971, the survey began on May 28 and ended on June 22; of a total of 26 days, 8 days were lost on account of the weather. In both years the survey was extended to include a strain network on top of the south dome, but the results of this survey will be given separately. This survey occupied a further 5 days on the average. In late June the divide snow usually contains free water, and the instrument set-ups become relatively unstable because of the settling of the tripod. Therefore the ice-cap survey should be finished before the end of June.

In 1970, the survey points were occupied according to the order in which they were set out, so that about 7 days had elapsed before the pole was assumed fixed within the ice. The survey was done in 1-day sections (Fig. 3) usually taking from 6 to 8 hours to complete depending on the conditions. Immediately following the completion of a section (normally involving six stations and ten individual station occupations), tripods were erected and centred at stations involved in the next section. In this way the tripods, having been set on wooden blocks buried more than 0.5 m below the snow surface, stabilized overnight.

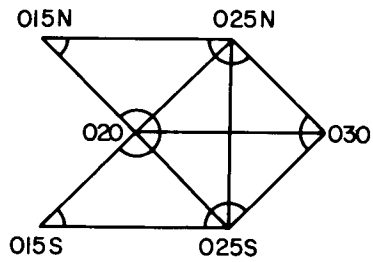

Figure 3. Typical daily survey section.

Angles at each station were measured by taking sets of direct and reverse readings until the spread of three sets was less than 5″ (5 seconds) of arc. Individual readings were made to 1″ (arc). On the average, six stations per day were completed. Triangular misclosures within the 1-day section were not usually permitted to exceed 10″ (arc), otherwise individual angle readings were repeated to supplement the original observations. This was not strictly enforced in 1970 because of time restrictions. Three readings taken in 1971 violated this criterion, but could not be repeated for several days because of poor visibility constraints. Ice deformation during this time contributed to the misclosure. Histograms of the angular misclosures for 1970 and 1971 are given in Figure 4. Simultaneous reciprocal vertical angles between stations were observed until three individual sets gave an angular spread of less than 10″ (arc). Slope distances were

measured in one direction using only the Distomat. Readings were taken until six values gave a spread of less than 3 cm. The distances from the bedrock stations A and B to the lowest ice-cap stations were measured with a Tellurometer.

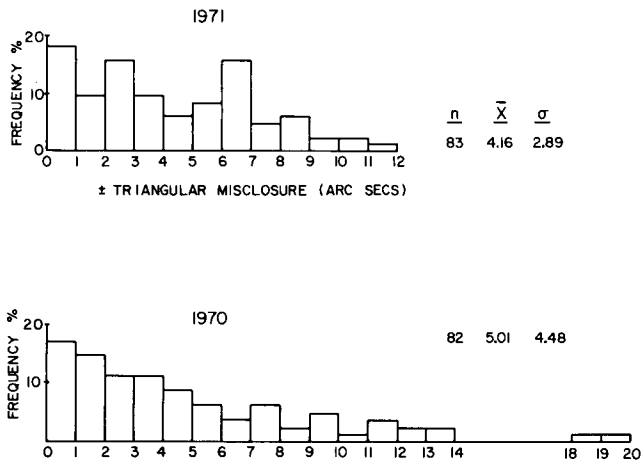

Figure 4. Histograms of triangular misclosure before adjustment where n = number of observations, $\bar{X}$ = mean, σ = standard deviation.

Tellurometer lines were measured using seven fine readings. All distances were corrected for temperature and pressure in the usual way.

ACCURACY

As suggested by the histograms in Figure 4, the angular measurements made in 1971 show an improvement over the 1970 measurements. The 1971 mean angular misclosure results in an average adjustment of about 1.4″ per angle.

Distances measured with the Distomat have a standard error of ±1.5 cm. For the lengths involved this represents an accuracy of from $\pm 1.5 \times 10^{-5}$ to $\pm 3 \times 10^{-5}$. For the distances measured with the Tellurometers the corresponding accuracy is $\pm 1 \times 10^{-5}$ for lines up to 6000 m.

DATA REDUCTION

Horizontal and Vertical Control

Elevation differences between stations were computed from the observed vertical angles (which, because they are simultaneous, allow the curvature and refraction terms to be eliminated by averaging) and the slope distances. These elevation differences were adjusted by least squares using the computer program LEVELOB (Peterson, unpublished) to obtain the adjusted values of the station elevations. Using these elevations, all slope distances were reduced to horizontal sea level distances.

The sea level lengths and the horizontal angles were then used in a least squares adjustment program GALS (Geodetic Adjustment by Least Squares) developed by the Geodetic Survey, Department of Energy, Mines and Resources. This program computes the adjusted geographic positions for each survey point. The co-ordinates for the fixed points A, B have been assumed from the results of a previous survey in 1966 by Henderson.

In the GALS program the relative weighting of angles and distances (inversely proportional to the variance of the observations) is generally important because of the influence of the weights on the computational position accuracy of the stations. Several adjustments were carried out before deciding on a suitable set of relative weights for the lengths and angles.

This procedure was implemented separately on the 1970 and 1971 sets of observations and the final geographic co-ordinates were converted to 6° UTM co-ordinates.

To obtain correct velocities, the sea level distances were converted to corresponding lengths at the actual station elevations. In practice, it was sufficient and simpler to recalculate co-ordinates and distances at a mean elevation for the survey of 700 m asl. Any scale change introduced by the use of the UTM system is assumed to be negligible over the distance of the traverse.

The results of these procedures are two separate sets of co-ordinates $(x^i_{0j}, y^i_{0j}, z^i_{0j})$; $(x^i_{1j}, y^i_{1j}, z^i_{1j})$ (where i = station number, j = 1,2 . . . trial number, 0 subscript is initial survey, and 1 subscript is final survey) applying, by hypothesis, at two times—$\bar{T}_0$ for the initial survey and $\bar{T}_1$ for the final survey. These times are taken arbitrarily to be on the day midpoint in time for each survey. Since the result of the actual survey is a series of stepped traverses (Fig. 5) caused by the time differences between the 1-day sections, these co-ordinates represent a first approximation only to the actual values that would apply at the time $\bar{T}_0$ and at the time $\bar{T}_1$.

Velocity Determinations Including Position Adjustment to Epoch (Specified Instant)

A program VELS does the following operations:

a) Computation of the apparent velocity components u^i_j, v^i_j, w^i_j in the directions x, y, z where x = latitude, y = longitude, z = elevation (Fig. 1) from:

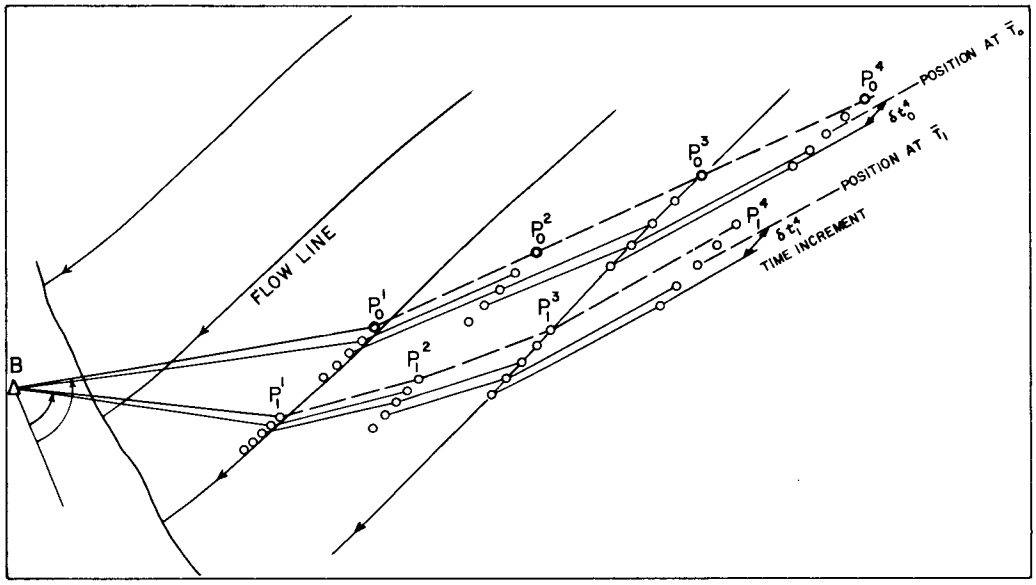

Figure 5. Simplified concept of the stepped traverse.

$$u_j^i = \frac{\left(x_{1j}^i\right) - \left(x_{0j}^i\right)}{\Delta\bar{T}}$$

$$v_j^i = \frac{\left(y_{1j}^i\right) - \left(y_{0j}^i\right)}{\Delta\bar{T}} \qquad (1)$$

$$w_j^i = \frac{\left(z_{1j}^i\right) - \left(z_{0j}^i\right)}{\Delta\bar{T}}$$

where $\Delta\bar{T} = \bar{T}_1 - \bar{T}_0$.

b) Determination of the time differences, δt, between the actual time a station observation was made and $\bar{T}_k$ ($k = 0$ for the initial survey and $k = 1$ for the final survey). For either survey, if T_k^i is the actual time of observation for a point P^i, then:

$$\delta t_k^i = \bar{T}_k - T_k^i$$

and the displacement components are:

$$\pm\delta x_{k,j}^i = u_j^i\,\delta t_k^i$$

$$\pm\delta y_{k,j}^i = v_j^i\,\delta t_k^i \qquad (k = 0, 1) \qquad (2)$$

$$\pm\delta z_{k,j}^i = w_j^i\,\delta t_k^i$$

where the sign depends on whether the time T_k^i is before or after $\bar{T}_k$.

c) Determination of the new co-ordinates of the point P^i, which then become:

$$x_{k,j+1}^i = x_{k,j}^i \pm \delta x_{k,j}^i$$

$$y_{k,j+1}^i = y_{k,j}^i \pm \delta y_{k,j}^i \qquad (k = 0, 1) \qquad (3)$$

$$z_{k,j+1}^i = z_{k,j}^i \pm \delta z_{k,j}^i.$$

d) Recalculation of the velocity components using equations (1) where j is put equal to $j + 1$.

Equations (2) in step (b) are then used to calculate the new displacement components with $j = j + 1$.

The iteration represented by steps (a) to (c) can be stopped at step (c) when:

$$x_{k,j+1}^i = x_{k,j}^i$$

$$y_{k,j+1}^i = y_{k,j}^i$$

$$z_{k,j+1}^i = z_{k,j}^i$$

consistent with the accuracy of the data. This was achieved at a value of $j = 5$.

ACCURACY OF RESULTS

From the results of the GALS output for 1970 and 1971, means and standard deviations for the residuals of lengths and angles are shown in Table 2. This provides a measure of the accuracy of the original data, and the severity of the assumption of simultaneity.

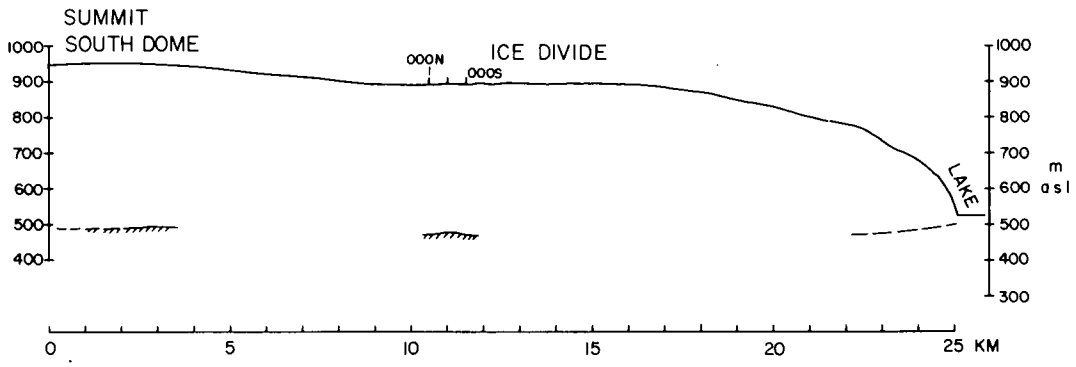

Figure 6. Profile from the summit of the south dome to the margin along the divide. Ice depths are from Jones (1972) and Jones and O'Neil (unpublished data).

Table 2. Statistics on Length and Angular Adjustment (length adjustment in metres, angle adjustment in seconds)

Quantity	Instrument	1970			1971		
		$\bar{X}$	s	n	$\bar{X}$	s	n
For lengths involving only A and B	Telluro-meter MRA-3	0.0345	0.0200	4	0.0062	0.0028	5
For lengths involving points only on the ice cap	Wild DI-10	0.0061	0.0049	103	0.0053	0.0038	104
Angles	Wild T2	2.4	2.06	181	2.8	2.4	174

Note: $\bar{X}$ = mean
s = standard deviation
n = number of values

Relative angular changes between individual diamonds in the network do not exceed about 1" (arc) per day in conjunction with lines stretching or contracting up to 3 mm per day, principally in the direction of the long axis of the network. The lowest poles in the network are only moving in the order of 1 cm per day, in the direction of the long axis of the network.

It is therefore justified, from a practical standpoint, to adjust the whole network as if the observations were all done simultaneously, since the adjustments done in one section rapidly become less dependent on the adjustments made in another section as the latter becomes more remote in the adjustment sequence. The subsequent iterative adjustment of stations to epoch should not, in principle, reduce the degree of accuracy obtained previously; that is, the final positions (reduced to epoch) can still be quoted with an error as determined by GALS initially. The adjustments of stations to epoch involve displacements ranging up to 3% of the total annual movement.

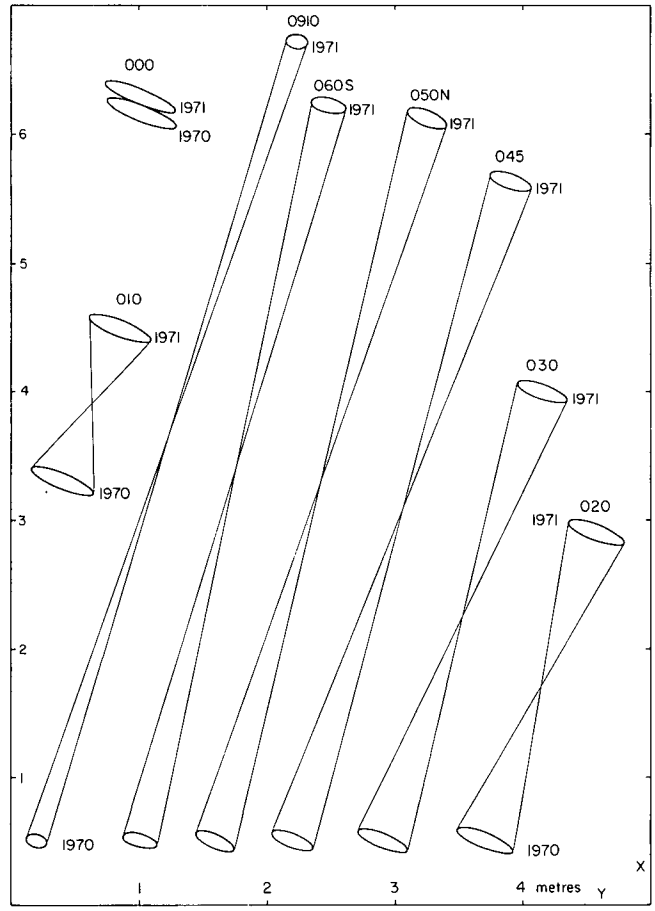

Figure 7. Error ellipses obtained from the adjustment program GALS for selected stations–relative to the fixed point A (Fig. 1). Relative co-ordinates are used but orientations are true. The possible error in the ice flow vectors can thus be seen.

VELOCITY RESULTS

Program VELS outputs the final velocity components u^i, v^i, w^i in the directions (Fig. 1) x—horizontal-north, y—horizontal-west and z—vertical, and the resultant velocity, at the points P^i. Table 3 shows values of the horizontal components of flow. It is seen that the requirement for the horizontal flow rate to be small or zero in the region of divide stations 000N, 000, 000S can be met; hence we have an independent check on the reliability of the velocity results. Since the divide is not continuously level, containing local humps (Fig. 6), some flow along and parallel to the divide is expected. It will be shown later, however, that we are able to isolate a point of zero horizontal flow rate, lying 149 m to the northeast of 000S. Figure 7 gives the error ellipses obtained from the GALS program applying at the 1970 and 1971 positions for 000, 010, 020, 030, 045, 050N, 060S, 0910, all relative to A. These ellipses, plotted on the same grid for comparison and convenience, form the basis of the probable errors in the resultant horizontal flow rate components given in Table 3.

The second part of the VELS program uses the General Purpose Contouring Program (GPCP). An ice

Table 3. Horizontal Components of Ice Flow Rate (m a^{-1})

Data point P^i (station)	u^i	v^i	Resultant horizontal velocity component $\sqrt{(u^i)^2+(v^i)^2}$	± error	Bearing from north (degrees)	± error	Remarks
0975 N	3.423	-1.485	3.731		23.447		Northeasterly flow
0975 S	1.998	-0.633	2.096		17.573		
0975	3.936	-1.634	4.262		22.546		
09425 N	5.381	-2.079	5.769		21.125		
09425 S	5.293	-1.735	5.571		18.151		
0910	6.229	-2.028	6.550	±0.10	18.032	±1.5°	
0875 N	6.517	-2.008	6.820		17.128		
0875 S	6.424	-1.632	6.628		14.258		
0840	6.611	-1.705	6.646		14.465		
08125 N	6.621	-1.776	6.856		15.014		
08125 S	6.558	-1.648	6.762		14.106		
0785	6.610	-1.679	6.819	±0.11	14.252	±2.0°	
0755 N	6.525	-1.664	6.734		14.307		
0755 S	6.465	-1.586	6.657		13.787		
0725	6.417	-1.594	6.612		13.952		
06875 N	6.284	-1.578	6.479		14.095		
06875 S	6.256	-1.550	6.445		13.916		
065	6.240	-1.561	6.433	±0.11	14.043	±2.6°	
060 N	6.002	-1.568	6.204		14.642		
060 S	5.729	-1.479	5.917	±0.11	14.471	±2.7°	
055	5.770	-1.547	5.974		15.011		
050 N	5.635	-1.654	5.873	±0.10	16.354	±3.0°	
050 S	5.267	-1.628	5.513		17.177		
045	5.141	-1.697	5.414	±0.11	18.263	±3.5°	
040 N	4.719	-1.580	4.977	±0.11	18.513	±4.0°	
040 S	4.603	-1.606	4.875		19.240		
035 N	4.177	-1.434	4.416		18.892		
035	4.137	-1.488	4.397		19.779		
035 S	4.056	-1.444	4.305		19.599		
030	3.498	-1.250	3.714	±0.11	19.662	±6.25°	
025 N	3.106	-1.049	3.279		18.654		
025 S	2.865	-1.070	3.058		20.472		
020	2.402	-0.880	2.559	±0.11	20.117	±10°	
015 N	1.893	-0.680	2.011		19.774		
015 S	1.783	-0.615	1.886		19.031		
010	1.190	-0.449	1.272	±0.12	20.669	±22.5°	
005 N	0.730	-0.286	0.784		21.403		
005 S	0.565	-0.151	0.585		14.963		
005	0.686	-0.230	0.723		18.514		
000 N	-0.008	-0.118	0.118		93.744		
000	-0.129	-0.011	-0.130	±0.3	175.109	±50°	Southwesterly flow
000 S	-0.215	0.043	-0.219		191.394		
005 W	-0.968	0.216	-0.991		192.562		

surface contour map is produced using the station elevation data and known pole heights. Slopes at centre-line stations were determined by levelling traverses. Values of the surface slope of the ice α^i (parallel to the flow line) are obtained at points P^i. The "true" vertical velocity component of the pole and hence the ice, w^{i*}, is given by:

$$w^{i*} = w^i \pm [(u^i)^2 + (v^i)^2]^{1/2} \cdot \tan \alpha^i \qquad (4)$$

where the negative sign applies when $w^i \cdot \Delta\overline{T}$ falls below the horizontal plane through the top of the initial pole position, and the positive sign applies when $w^i \cdot \Delta\overline{T}$ rises above the horizontal plane. The former case applies in the accumulation area when $w^i > [(u^i)^2 + (v^i)^2]^{1/2} \cdot \tan \alpha^i$. The latter case applies in the ablation area. Values of w^{i*} are given in Table 4 together with the errors determined from the residual appearing in the output of the LEVELOB program. As with the horizontal velocities, we have assumed that the adjustments to epoch have not affected the error in the original elevation values.

Table 4. Vertical Components of Ice Flow Rate (m a^{-1})

Data point P^i (station)	w^i	± error	w^{i*}	± error	$w_\perp^{i*}$ component perpendicular to ice surface	Angle of emergence (+) or descent (−) from horizontal $\tan^{-1}(w^{i*}/\sqrt{(u^i)^2+(v^i)^2})$		Resultant ice flow rate vector $\sqrt{(u^i)^2+(v^i)^2+(w^{i*})^2}$	
0975 N	0.512	±0.015	0.851	±0.03	0.847	+12.8°	±0.5°	3.827	±0.10
0975 S	0.382	±0.016	0.586	±0.03	0.583	15.6		2.176	
0975	0.613	±0.023	1.036	±0.04	1.031	13.7		4.386	
09425 N	0.522	±0.026	1.062	±0.05	1.057	10.4		5.866	
09425 S	0.402	±0.025	0.924	±0.05	0.920	9.4		5.647	
0910	0.199	±0.026	0.737	±0.05	0.734	6.4		6.591	
0875 N	0.122	±0.029	0.689	±0.05	0.687	5.8		6.855	
0875 S	0.275	±0.029	0.827	±0.05	0.824	7.1		6.679	±0.11
0840	0.105	±0.031	0.597	±0.05	0.602	5.1	±0.5°	6.673	±0.11
08125 N	0.129	±0.034	0.572	±0.054	0.608	4.8		6.880	
08125 S	0.003	±0.034	0.440	±0.053	0.458	3.7		6.776	
0785	0.073	±0.035	0.476	±0.055	0.493	4.0		6.836	
0755 N	0.091	±0.038	0.444	±0.055	0.460	3.8		6.749	
0755 S	0.111	±0.038	0.460	±0.055	0.496	+4.0		6.673	
0725	0.074	±0.039	0.388	±0.056	0.401	3.4		6.623	
06875 N	0.147	±0.044	0.427	±0.060	0.419	3.8	±0.6	6.493	±0.11
06875 S	0.166	±0.042	0.445	±0.058	$w_\perp^{i*} \approx w^{i*}$	4.0	±0.6°	6.460	±0.11
065	0.122	±0.043	0.375	±0.059		3.3		6.444	
060 N	0.121	±0.046	0.351	±0.060		3.2		6.214	
060 S	−0.013	±0.046	0.204	±0.060		2.0		5.921	
055	−0.012	±0.046	0.199	±0.060		1.9		5.977	
050 N	−0.130	±0.048	0.073	±0.062		0.7		5.873	
050 S	−0.115	±0.048	0.075	±0.062		0.8		5.514	
045	−0.001	±0.049	0.178	±0.062		+1.9	±0.6°	5.417	±0.11
040 N	−0.068	±0.051	0.088	±0.063	$w^{i*} \approx w_\perp^{i*}$	+1.0	±0.8°	4.978	±0.12
040 S	−0.160	±0.051	−0.044	±0.056		−0.1		4.875	
035 N	−0.159	±0.053	−0.032	±0.064		−0.6		4.416	
035	−0.153	±0.052	−0.026	±0.063		−0.4		4.397	
035 S	−0.147	±0.054	−0.027	±0.065		−0.4		4.305	
030	−0.145	±0.054	−0.051	±0.063		−0.8		3.714	
025 N	−0.235	±0.056	−0.163	±0.065		−2.8		3.283	
025 S	−0.215	±0.056	−0.151	±0.064		−2.8	±1.2°	3.061	±0.12
020	−0.229	±0.057	−0.178	±0.064	$w^{i*} \approx w_\perp^{i*}$	−3.9	±1.7°	2.565	±0.12
015 N	−0.288	±0.058	−0.246	±0.064		−7.1		2.027	
015 S	−0.262	±0.058	−0.222	±0.064		−6.9		1.900	
010	−0.280	±0.059	−0.254	±0.064		−11.3		1.297	
005 N	−0.305	±0.060	−0.293	±0.064		−20.6		0.838	
005 S	−0.270	±0.061	−0.262	±0.064		−24.3		0.642	
005	−0.298	±0.061	−0.286	±0.064		−21.6		0.776	
000 N	−0.308	±0.062	−0.308	±0.063		−69.0	±20°	0.330	±0.11
000	−0.288	±0.061	−0.287	±0.062		−65.6	±25°	0.315	±0.24
000 S	−0.285	±0.062	−0.285	±0.064	$w^{i*} \approx w_\perp^{i*}$	−52.5		0.359	
005 W	−0.289	±0.064	−0.272	±0.064		−15.3	±5°	1.028	±0.20

Next a horizontal velocity (component) grid is established for the purposes of deriving a) ice flow lines and b) velocity gradients for strain rate determination.

Using program FLOW, flow lines are generated by selecting a suitable starting point near the divide where there is a finite flow rate. The program computes distance moved using a time increment of one year and interpolates from the grid to obtain (u, v) values for developing the flow line. Several flow lines were produced in this way on the Calcomp plotter (Fig. 8).

Velocity gradient values determined previously are now used in a program RATE, which computes principal strain rates at each data point using the components of the strain rate tensor:

$$\dot{\epsilon}_{xx} = \frac{\partial u^i}{\partial x} \qquad \dot{\epsilon}_{yy} = \frac{\partial v^i}{\partial y}$$

$$\dot{\gamma}_{xy} = \frac{\partial u^i}{\partial y} + \frac{\partial v^i}{\partial x} \qquad (\text{note } \dot{\epsilon}_{xy} = \tfrac{1}{2}\dot{\gamma}_{xy}). \tag{5}$$

The principal strain rates $\dot{\epsilon}_1$ and $\dot{\epsilon}_2$ and their orientations are then computed using the equations of Nye (1959). It should be remembered that these strain rates apply within a horizontal plane lying at the surface of the glacier. Table 5 gives the values at each data point P^i.

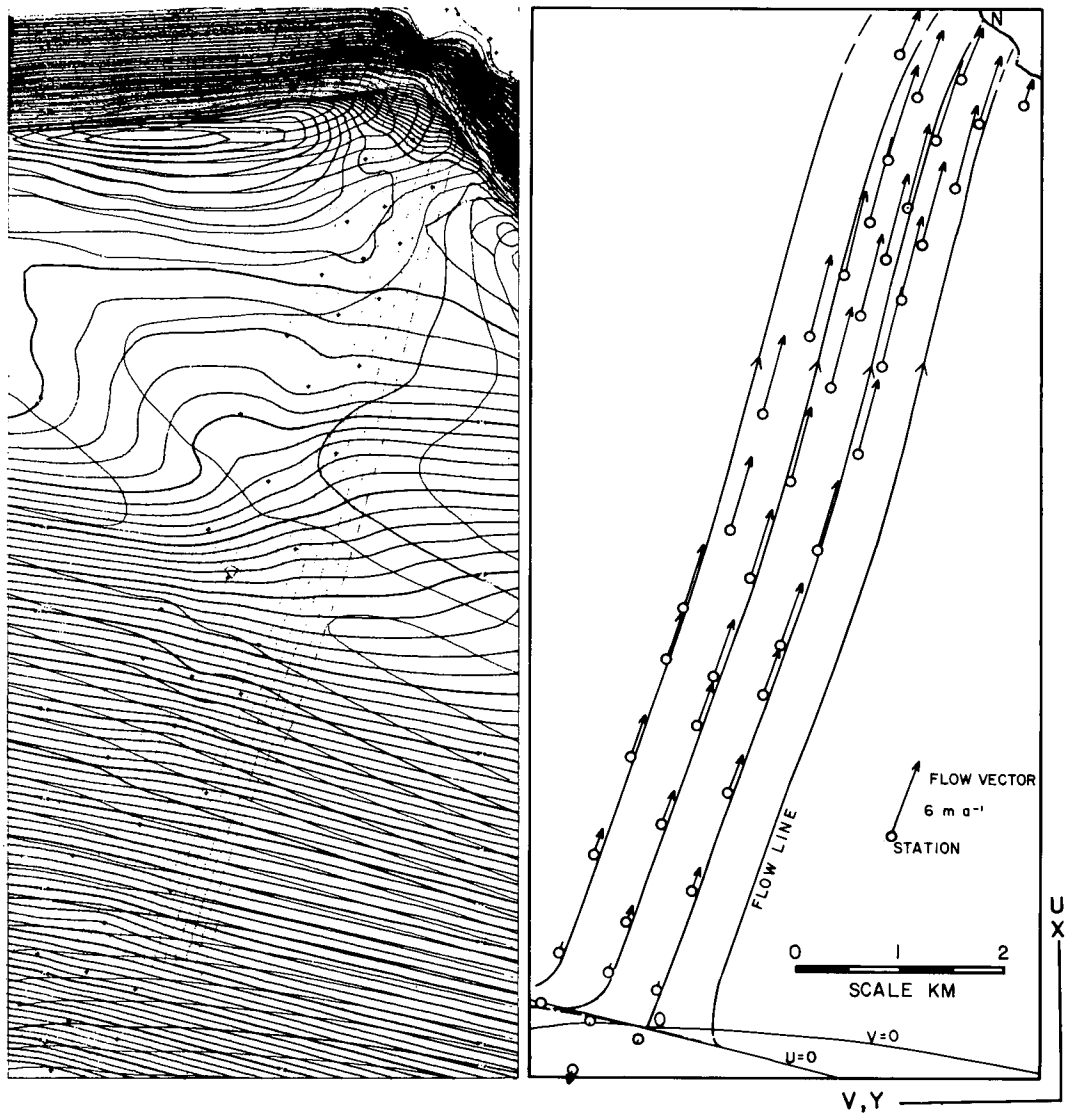

Figure 8. (a) Plot of velocity components u,v and flow lines generated from them; (b) flow vector directions and flow lines as generated in the previous plot by the program FLOW. Flow line ON begins where u,v = 0.

VERTICAL PROFILE FOR FLOW ANALYSIS

The flow line ON (Fig. 8), generated from near the point of zero flow rate and passing through it, defines a convenient profile (Fig. 9) along which variations of strain rate and stress (Fig. 10) are next examined. Ice thicknesses along the profile (Fig. 9) have been determined by preparing an isopach map using the data of Jones (1972). Basal temperatures have been computed using the simple model of Jenssen and Radok (1963); see also Holdsworth (1973a). Principal strain rates (Fig. 11) are seen to be acting nearly parallel and perpendicular to the flow line. Deviations up to 3° (arc) occur.

Co-ordinate System

Adopting a new right-handed rectangular co-ordinate system where x is in the direction of the flow line, y is transverse to it and z is perpendicular to the glacier surface (z is positive downward), in which lies the origin, we take $\dot{\epsilon}_1 \cong \dot{\epsilon}_{xx}$ and $\dot{\epsilon}_2 \cong \dot{\epsilon}_{yy}$.

Table 5. Principal Strain Rates at Data Points

Data point P^i (station)	$\dot{\epsilon}_1$ (x $10^{-3}a^{-1}$)	$\dot{\epsilon}_2$ (x $10^{-3}a^{-1}$)	Bearing of $\dot{\epsilon}_1$ direction from north	Remarks
0975N	−7.04 ±0.10	+0.10 ±0.10	13.4 ±3°	
0975S	6.94	+0.44	32.2	Variable due to shallow
0975	6.16	−0.38	26.8	ice and structure
09425N	4.37	−0.26	18.5	
09425S	5.83	−0.32	27.5	
0910	2.50	−0.35	21.5	
0875N	0.62	−0.23	34.1	
0875S	0.86	−0.37		
0840	−0.03	0.29	16.9	
08125N	+0.10	0.21	11.3	
08125S	0.07	0.19	15.3	
0785	0.12	0.17	13.6	
0755N	0.29	0.07	12.8	
0755S	0.27	0.12	13.5	
0725	0.30	0.07	13.9	
06875N	0.35	0.02	14.5	
06875S	0.38	0.05	9.2	
065	0.37	0.05	3.9	
060N	0.44	0.03		Bearings unreliable
060S	0.56	0.14		
055	0.54	0.08		
050N	0.96	−0.02		
050S	0.72	−0.01		
045	0.97	+0.03		
040N	1.08 ±0.11	0.00 ±0.11	10.2	
040S	+1.01 ±0.11	+0.08 ±0.10	13.5 ±2°	
035N	1.13	0.06	13.9	
035	1.18	0.05	15.2	
035S	1.17	0.04	15.6	
030	1.23	0.07	15.2	
025N	1.21	0.09	13.6	
025S	1.21	0.07	14.9	
020	1.23	+0.03	15.5	
015N	1.25	−0.01	15.8	
015S	1.25	−0.04	17.5	
010	1.29	0.05	15.8	
005N	1.45	0.06	12.8	
005S	1.48	0.12	15.9	
005	1.51	0.08	13.9	
000N	1.52	0.12	12.8±*	*divide region-deviation
000	1.57	0.10	14.3 (194.3)±2°	of $\dot{\epsilon}_1$, from flow lines
000S	1.55	0.07	14.5 (194.5)±2°	(Fig. 15)
005W	+1.66 ±0.11	−0.10 ±0.10	14.6 (194.6)±2°	
			(cf. col. 5) Table 3	

Note: Sign convention: −compressive
+extensive
Contrary to normal practice $\dot{\epsilon}_1$ has been taken as the principal strain rate closest to the x – direction, along the flow line.

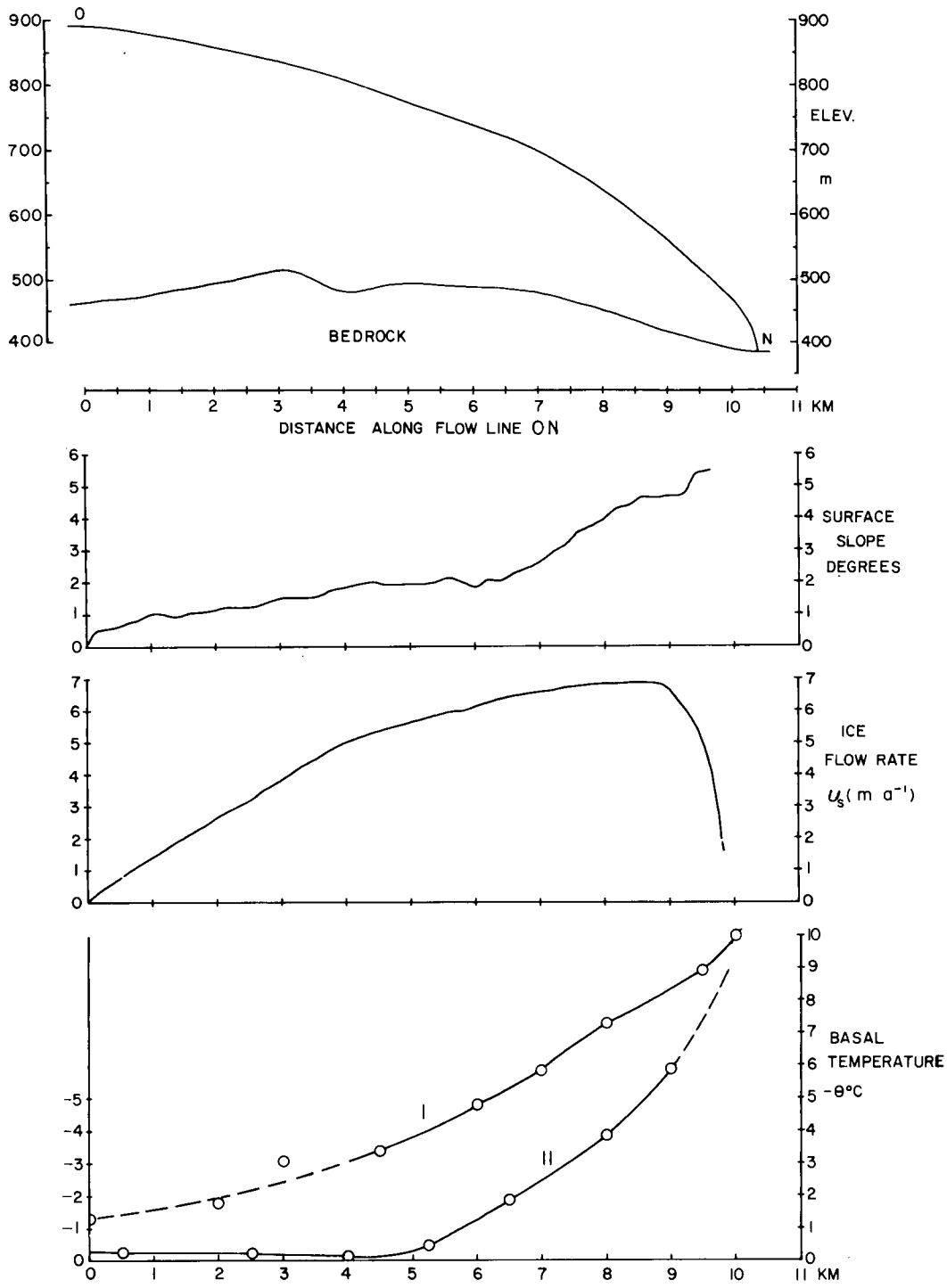

Figure 9. Ice-cap longitudinal profile along the flow line ON. Variations in surface slope, surface velocity and theoretical basal temperatures are also given. In the latter case, Curve I corresponds to a geothermal gradient of $0.02^{\circ}C\ m^{-1}$; Curve II corresponds to a geothermal gradient of $0.0344^{\circ}C\ m^{-1}$ (Holdsworth, 1973a).

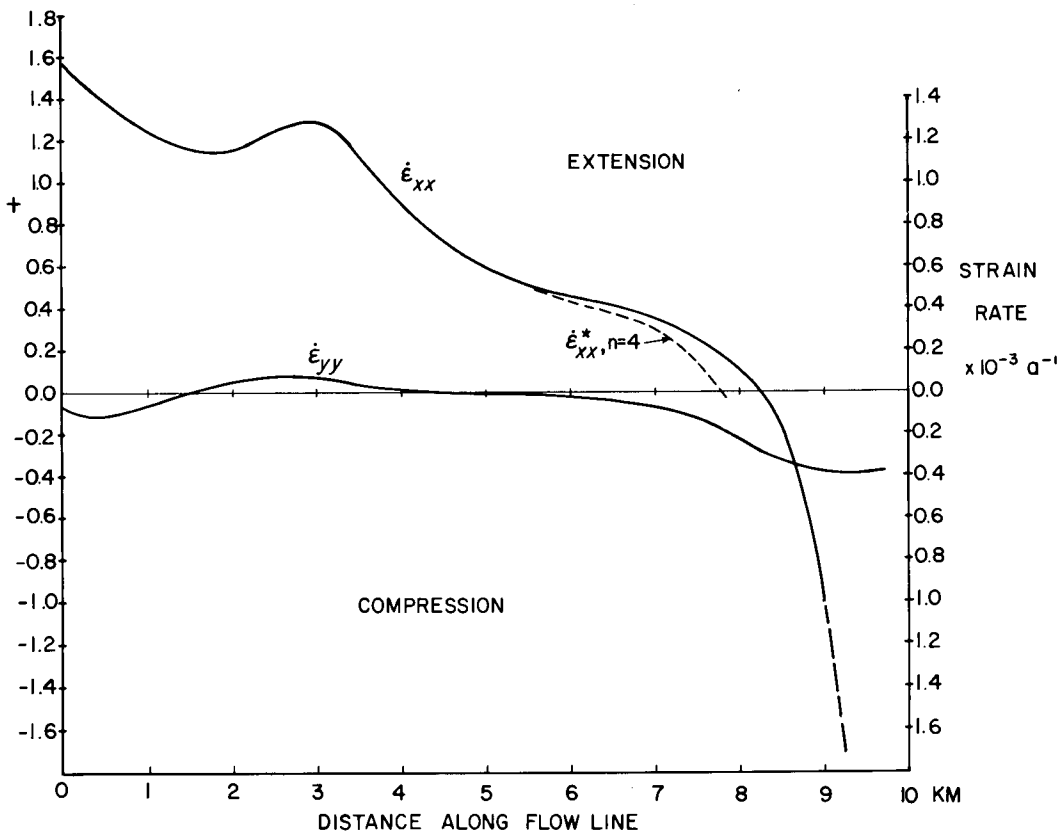

Figure 10. Variation of strain rate components $\dot{\epsilon}_{xx}$ and $\dot{\epsilon}_{yy}$ along the flow line ON.

Flow Law

We assume a flow law of the type (Nye, 1957):

$$\dot{\epsilon}_{ij} = \lambda \sigma'_{ij} \tag{6}$$

where $\dot{\epsilon}_{ij}$ and σ'_{ij} are the strain rate and stress deviator components, respectively, and i, j are now the symbols for repeated subscripts:

$$i, j = x, y, z\,.$$

The quantity

$$\lambda = B^{-n}\tau^{n-1}$$

where B is a factor dependent on crystal size and orientation, impurities in the ice, and temperature. As a function of the latter, B is usually written:

$$B = B_0 e^{-\nu\theta} \tag{7}$$

where B_0 is a constant under uniform crystal properties; ν is a factor $= \frac{k}{n}$; $k \approx 0.1$ (Budd, 1969) and θ is the (negative) temperature in °C; n is an exponent which seems to vary with stress; and τ is the "effective stress" defined by:

$$2\tau^2 = \sigma'_{ij} \cdot \sigma'_{ij}\,. \tag{8}$$

The "effective strain rate" is defined by:

$$2\dot{\epsilon}^2 = \dot{\epsilon}_{ij} \cdot \dot{\epsilon}_{ij}\,.$$

Since the strain rate data show that the transverse component $\dot{\epsilon}_2$ is an order of magnitude less than $\dot{\epsilon}_1$ (up to $x =$ 7.5 km), we make the simplifying assumption that:

$$\dot{\epsilon}_{yy} \approx 0$$

and the incompressibility condition then gives:

$$\dot{\epsilon}_{xx} = -\dot{\epsilon}_{zz}\,.$$

Consequently, from (6):

$$\sigma'_{xx} = -\sigma'_{zz}\,. \tag{9}$$

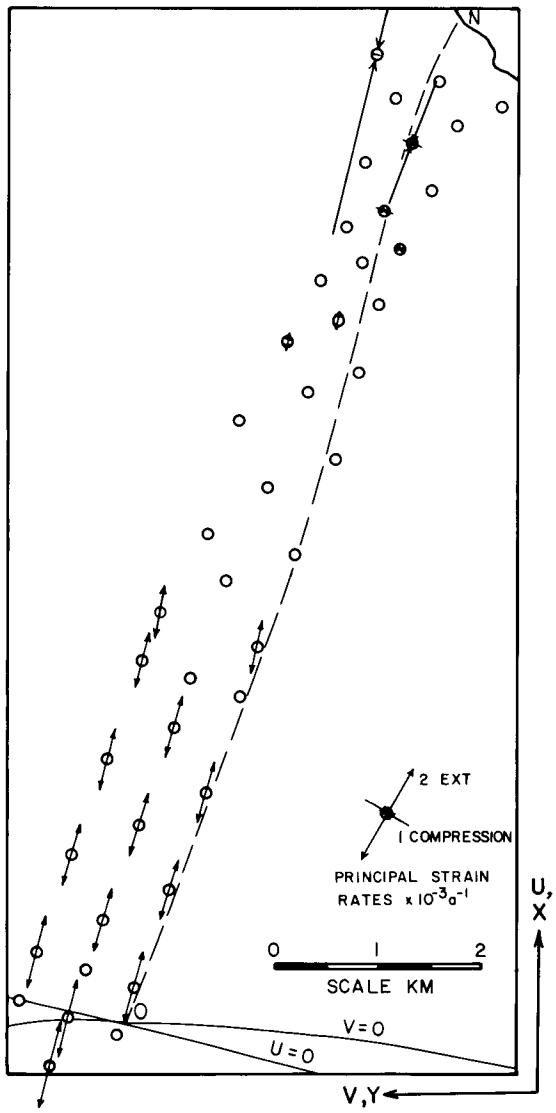

Figure 11. Principal strain rate directions in relation to flow line ON. See Table 5 for detailed values. Central values are small and orientations unreliable.

Determination of Flow Law Constants

From the flow law, Equation (6) and the equations of motion, Budd (1969, p. 119) has derived the following equation which accounts for deformation in three dimensions along a flow line in the absence of basal slip:

$$-\frac{\partial}{\partial x}\left(\bar{H}\bar{B}_1\,\dot{\epsilon}_{xx}^{*\,1/\bar{n}_1}\right) \approx \frac{1}{2}\rho_i g\bar{H}\bar{\alpha} - \frac{B_2}{2}\left(\frac{n_2+1}{2}\cdot\frac{u_s}{H}\right)^{1/n_2} - \frac{\rho_i g}{6}\cdot\frac{\partial^2}{\partial x^2}\,\bar{\alpha}\,\bar{H}^3 \tag{10}$$

where $\bar{H}$ is the average ice thickness and $\bar{\alpha}$ is the average surface slope smoothed over 2-kilometre distances and $\bar{B}_1$ and $\bar{n}_1$ are the flow law parameters averaged over the thickness of the glacier. B_2 and n_2 are the average values for the basal zone (Budd, 1969, p. 118), u_s is the surface longitudinal flow rate, ρ_i is the average density of the ice and g is the acceleration of gravity.

Following Budd (1969):

$$\dot{\epsilon}_{xx}^{*} = \phi\dot{\epsilon}_{xx}$$

where

$$\phi = \left(1+\frac{r}{2}\right)\left[1+3\left(\frac{r}{2+r}\right)^2\right]^{-(n-1)/2}$$

and

$$r = \dot{\epsilon}_{yy}/\dot{\epsilon}_{xx}\,.$$

Assuming B can be written in the form of Equation (7), Equation (10) may be rewritten:

$$\gamma\,\rho_i g\,\bar{H}\bar{\alpha} + 2\gamma\frac{\partial}{\partial x}\left(\bar{H}\bar{B}_{0,1}\,e^{-\nu\theta}\,\dot{\epsilon}_{xx}^{*\,1/n_1}\right) = \left(e^{-k\theta}\cdot\frac{u_s}{H}\right)^{1/n_2} + \frac{\gamma}{3}\rho_i g\frac{\partial^2}{\partial x^2}\,\bar{\alpha}\bar{H}^3 \tag{11}$$

where

$$\gamma = \left(\frac{2}{n_2+1}\right)^{1/n_2} \Big/ B_{0,2}.$$

To solve Equation (11) for B and n it is necessary to make the following approximations by putting:

$$n_1 \simeq n_2 \simeq n$$

$$B_{0,1} = B_{0,2} = B_0\,.$$

We now examine the term containing $\frac{\partial^2}{\partial x^2}\,(\bar{\alpha}\bar{H}^3)$. Figure 12 shows a plot of $\bar{\alpha}\bar{H}^3$ with actual values and smoothed values. Averaged over the interval $1 < x \leqslant 8$ km (in which we are seeking to obtain average values of B and n) it can be seen that $\frac{\partial}{\partial x}\,(\bar{\alpha}\bar{H}^3) \approx$ constant. Therefore $\frac{\partial^2}{\partial x^2}\,(\alpha\bar{H}^3) \approx 0$, which is the general result reached by Budd (1969) when averaging over distances of 10 to 20 times the ice thickness. Equation (11) now simplifies to:

$$\left(\frac{2}{n+1}\right)^{1/n}\frac{\rho_i g}{B_0}\,\bar{H}\bar{\alpha} + 2\left(\frac{2}{n+1}\right)^{1/n}\frac{\partial}{\partial x}\left(\bar{H}e^{-\nu\theta}\,\dot{\epsilon}_{xx}^{*\,1/n}\right) = \left(\frac{u_s}{H}\,e^{-k\theta}\right)^{1/n}. \tag{12}$$

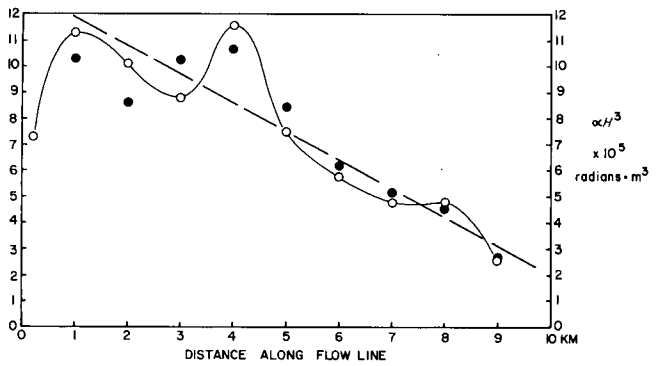

Figure 12. Plot of quantity $\bar{\alpha}\bar{H}^3$ versus distance along the flow line. Open circles–point values; closed circles–values smoothed over 2 km.

Initial trial values of $B_0 = 18.762$ MN m^{-2} s$^{0.265}$, and $n = 3.77$ were obtained by taking $\frac{\partial}{\partial x}(\bar{H}\, e^{-\nu\theta}\, \dot{\epsilon}_{xx}^{*\,1/n}) = 0$, and plotting $\bar{\alpha}\bar{H}$ versus $(\frac{u_s}{\bar{H}})e^{-k\theta}$ on log-log paper and obtaining the slope of the curve.

The subsequent procedure involves taking the $\left(\frac{u_s}{\bar{H}}\right)e^{-k\theta}$ values just obtained and plotting these against:

$$\xi\,\overline{H\alpha} + \psi\,\frac{\partial}{\partial x}\left(\bar{H}e^{-\nu\theta}\ \dot{\epsilon}_{xx}^{*\,1/n}\right)$$

where

$$\xi = \left(\frac{2}{n+1}\right)^{1/n} \rho_i g / B_0$$

and

$$\psi = 2\left(\frac{2}{n+1}\right)^{1/n}$$

to produce a better value of n. The iteration is stopped when the last value of n substituted equals the value obtained from the slope of the curve to within the accuracy of the fit. This also satisfies the solution for B_0.

Figure 13 represents a fourth iteration and yields a value of $n = 4.2 \pm 0.1$.

The lower line represents model I and the upper line model II of the basal temperature distribution (Fig. 9). In Figure 13, the lower line appears to have a slightly greater slope than the upper line (i.e., using the thermal model notations $n_{\mathrm{I}} > n_{\mathrm{II}}$) and this would agree with the relationship:

$$(1/B_{0\mathrm{I}})^{n_{\mathrm{I}}} = (1/B_{0\mathrm{II}})^{n_{\mathrm{II}}} \quad (B_{0\mathrm{II}} > B_{0\mathrm{I}})$$

obtained from the flow law. If we accept the values of:

$$B_{0\mathrm{I}} \approx 10.95 \text{ MN m}^{-2} \text{ s}^{1/4.2}$$

$$B_{0\mathrm{II}} \approx 12.85 \text{ MN m}^{-2} \text{ s}^{1/4.2}$$

obtained from the two lines in Figure 13 then:

$$n_{\mathrm{I}} / n_{\mathrm{II}} = 1.009$$

or, if we accept

$$n_{\mathrm{I}} = 4.2$$

then

$$n_{\mathrm{II}} = 4.16.$$

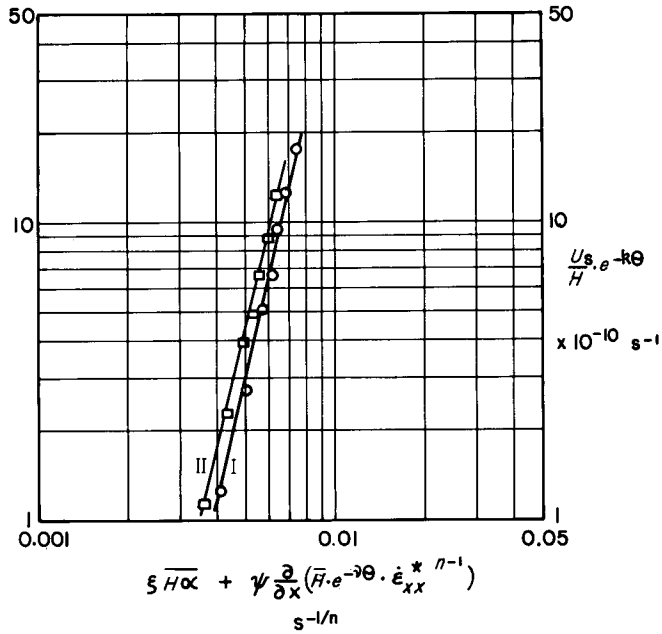

Figure 13. Plot of $u_s e^{-k\theta}/H$ versus $\xi\,\bar{H}\,\bar{\alpha} + \psi\,\frac{\partial}{\partial x}(\bar{H}e^{-\nu\theta}\dot{\epsilon}_{xx}^{*\,1/n})$. Curve I–temperature model I; Curve II–temperature model II.

This result is not meant to imply an increase of accuracy, but to reconcile the different values of B_0 obtained, and to show that moderate errors in assumed temperature values do not greatly influence n or B_0. Further we have ignored the possibility of basal slip which might be associated with the first half of model II, although this cannot be proven.

A mean value is given as:

$$B_0 = 11.9\ (\pm 1.0) \text{ MN m}^{-2} \text{ s}^{1/4.2}.$$

Calculation of Stresses

If the stresses σ'_{xx}, σ'_{zz} and σ_{xz} $(= \sigma_{zx})$ are finite and $\sigma'_{yy} = 0$ $(0 < x > 7.5$ km), then using Equations (8) and (9):

$$\tau = [(\sigma'_{xx})^2 + (\sigma_{zx})^2]^{1/2} \tag{13}$$

where the shear stress $\sigma_{zx} \approx \rho_i g\, z \sin \bar{\alpha}$ (14)

(ρ_i is the density of the ice, assumed uniform, and $\bar{\alpha}$ is the smoothed surface slope). The basal shear stress from Equation (14) is:

$$\sigma_{zx}|_b = \rho_i g \bar{H} \sin \bar{\alpha}$$

where $\bar{H}$ is the smoothed ice thicknesses.

Equation (6) may now be used with (13) and (14) to give:

$$\dot{\epsilon}_{xx} = B^{-n} [(\sigma'_{xx})^2 + (\sigma_{zx})^2]^{\frac{1}{2}(n-1)} \sigma'_{xx} \tag{15}$$

where $\dot{\epsilon}_{xx}$, σ'_{xx} B and n are assumed to vary with depth z. (B and n are taken to be about 11.9 MN m^{-2} s$^{0.238}$ and 4.2, respectively only in the *lower* part of the ice cap.)

Since the assumption of zero basal slip implies $\dot{\epsilon}_{xx}|_b = 0$ and hence by (6): $\sigma'_{xx}|_b = 0$ (at the bottom), we now make some simplifications:

a) Assume (Budd, 1969):

$$\bar{\dot{\epsilon}}_{xx} / \dot{\epsilon}_{xx}|_s = \bar{u} / u_s = R$$

where the subscript s denotes a surface value and the bar denotes an average value over the depth H. It may be readily shown that (for isothermal ice) $R = n + 1/n + 2$ and hence for the present case $R \approx 0.83$, very approximately.

b) It follows that $\bar{\sigma}'_{xx} \approx 0.83\, \sigma'_{xx}|_s$.

c) We assume that the $\bar{\sigma}'_{xx}$ value occurs at about the same depth as the $\bar{u}$ value, which is about $0.70H$ (again for isothermal ice).

Equation (15) is now used in which $\dot{\epsilon}_{xx}$ and σ'_{xx} take values of 83% of their surface values and σ_{zx} takes values appropriate to a depth of $z = 0.70H$. We assume that this is sufficiently deep within the ice for us to use the values of B and n derived previously.

Equation (15) has been solved for σ'_{xx} using an interval halving method and then τ has been calculated using Equation (13). These values, together with $\sigma_{zx}|_b$, are shown in Figure 14. The actual stresses appropriate for the

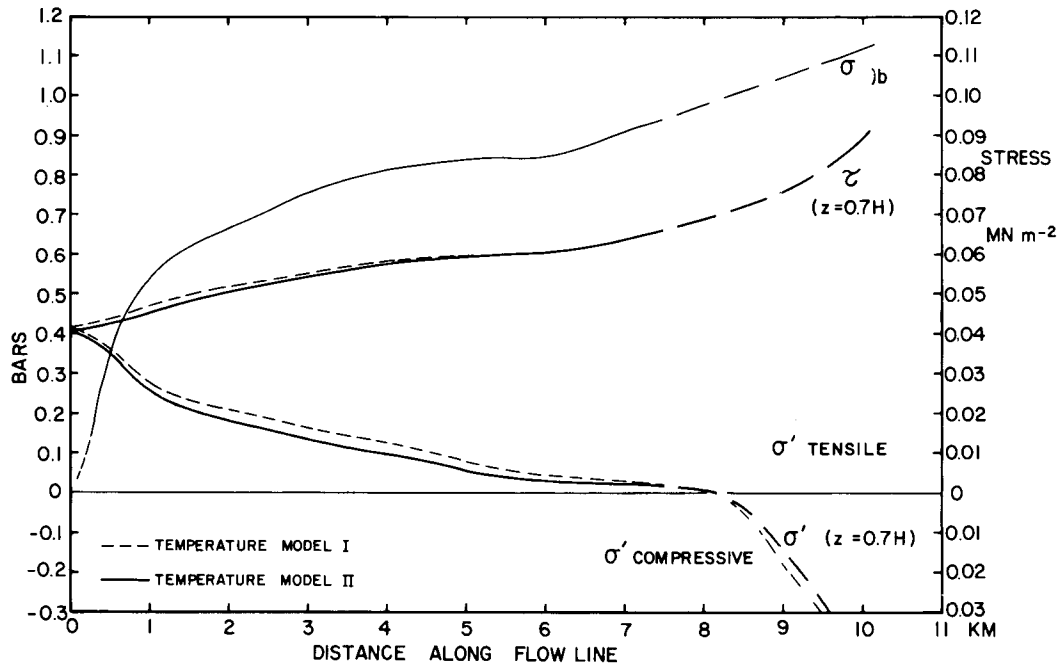

Figure 14. Variation of stresses at the base and at about $0.3H$ above the base along the flow line ON. Beyond $x = 7.5$ km variation is only approximate as $|\sigma'_{yy}|$ increases to become comparable to $|\sigma'_{xx}|$.

B and n values derived are thought to lie between the $\sigma_{zx}|_b$ $(=\tau_b)$ value and the value of τ which applies at about $0.70H$ below the surface.

DISCUSSION OF RESULTS

Survey Results

The result from the velocity data that a point could be found where u, v = 0 within 150 m of the "apparent" topographic divide (as determined by the profile of the snow surface) suggests that the velocity data are reliable within the limitations of the methods used. A combined open-traverse/triangulation/trilateration developed from station 000 to the top of the south dome was also completed in 1970 and 1971. Using the same methods of data reduction described, a zero horizontal velocity point was found to exist on the top of the dome, thus also giving a second independent check on the velocity and hence position determinations. These results will be reported elsewhere.

The error in velocities (Table 3) could account for the apparent displacement of the "dynamic divide" from the topographic divide (Fig. 15). The flow lines and principal strain rate directions in the region of the divide, however, are realistic, so there is a high probability that the displacement is real. *Assuming* that under *normal* steady-state conditions the point where u, v = 0 corresponds with the topographic divide, we suggest that to account for the present observation the divide is drifting to the northeast (compare Orvig, 1953; Løken and Andrews, 1966).

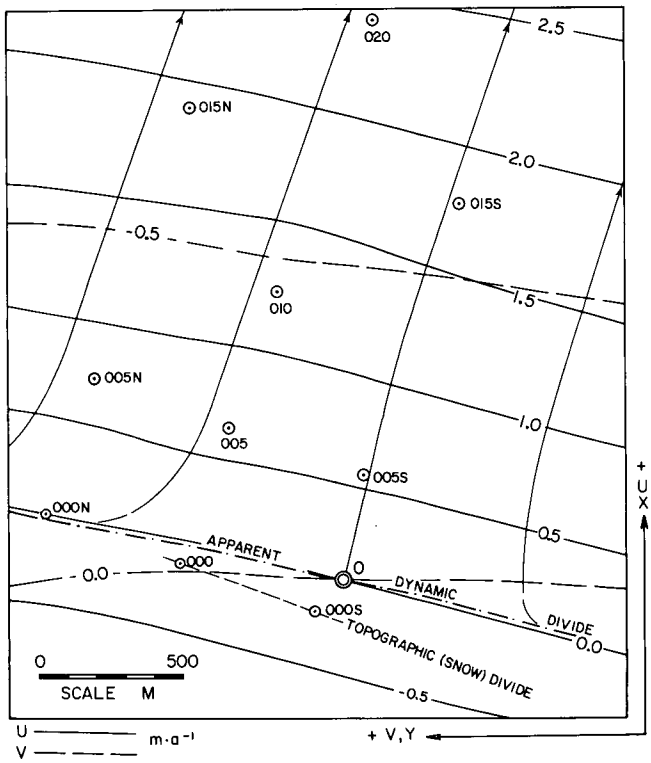

Figure 15. Divide region showing position of "apparent dynamic divide" and topographic divide.

The divide has been displaced about 5 km to the northeast, as the result of a surge of the southern part of the ice cap (Holdsworth, 1973a). Based on the possible times when the surge began, *average* divide displacement rates of from 26 m a^{-1} to 147 m a^{-1} are obtained. We do not expect such high values to apply *now*, as it is believed that the displacement rate decreases with time, being the greatest in the early stages of the surge phase.

Current Net Mass Balance and Vertical Ice Flow

Figure 16 shows that at the divide the mean annual accumulation of superimposed ice from 1970 to 1973 is about 0.386 ± 0.15 m a^{-1} (average density 900 kg m^{-3}). At the same location the vertically downward ice velocity is about −0.29 ± 0.06 m a^{-1}.

The average balance line occurs at about 690 m, whereas the elevation of zero flow rate perpendicular to the ice surface is about 810 m.

Ice emergence rate and ablation at the lower end of the network appear to be about 1.0 m a^{-1} and 0.8 m a^{-1}, respectively. Thus, dynamically, the ice cap seems to be reacting to a lower accumulation rate and higher ablation rate than are currently recorded. It should be noted, however, that aerial photographs taken in July 1961, show the divide almost stripped of snow and firn, indicating that the long-term average annual net balance may be lower than the value recorded in the interval 1970-73. The data of Løken and Sagar (1968) indicate a large variation in mass balance with respect to time, and it is felt that at least a decade of mass balance measurements should be made.

Flow Law Results

The values of n and B_0, derived from variation in the longitudinal dynamic properties of the ice cap, are *average* values applying in the stress range $0.05 < \tau < 0.1$ MN m^{-2} and in the basal temperature range from −0.277°C to −10°C. The effect of assuming $n_1 = n_2$; $B_{0,1} = B_{0,2}$ in Equation (11) is now discussed. The term affected is:

$$\frac{\psi}{B_{0,2}} \frac{\partial}{\partial x}\left(\overline{HB}_{0,1}\, e^{-\nu\theta}\, \dot{\varepsilon}_{xx}^{*\,1/n_1}\right) \qquad (16)$$

which is normally an order of magnitude smaller than the term $\xi\overline{H\alpha}$. In addition, the *gradient* value in (16) is not

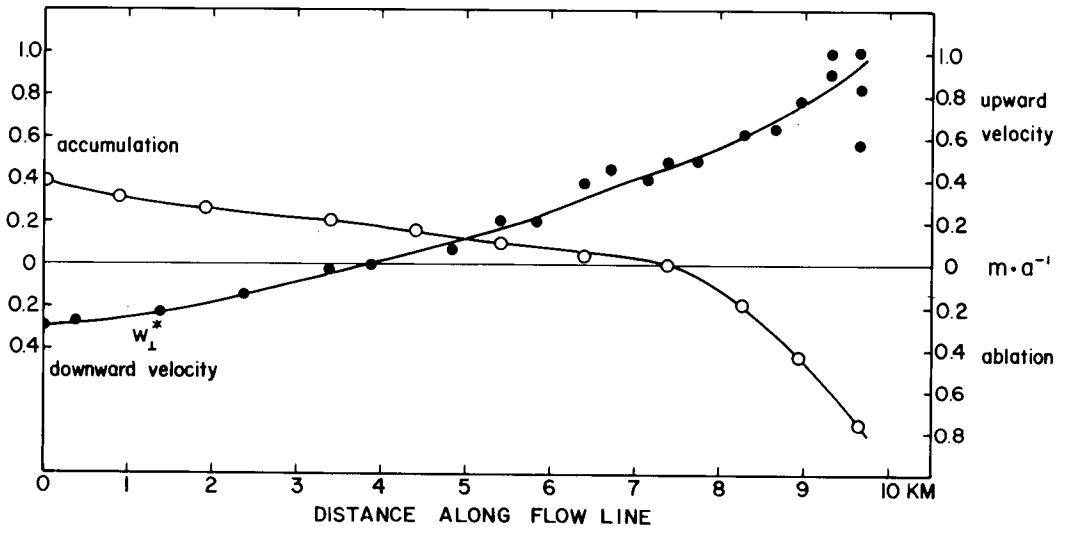

Figure 16. Plot of flow rate component perpendicular to the ice surface and smoothed accumulation/ablation data for 1970-73 period.

very sensitive to n_1. We expect that averaged over the *vertical* section the value of n_1 is less than the value found here for the basal region because, as Budd (1969) has shown, there is considerable evidence that n decreases with decreasing stress. Figure 17 shows that the gradient values actually decrease slightly as n takes values from 4.5 to 3.5.

Of greater importance is the ratio $B_{0,1}/B_{0,2} > 1$ which tends to increase the value of (16) shifting the lines in Figure 13 to the right, but has only a minor effect on the slope. Estimates for the actual value of $B_{0,1}$ are not available.

The results of this paper are a first step toward the calculation of vertical profiles of velocity and improved temperature profiles. More data are needed to decide whether the position of the present divide is stable or is still migrating as a result of a surge. Only then can the problem of calculating flow lines and the age of the ice be attempted realistically.

Results of Orvig and Ward

In the light of the present data, the recognition of the effects of a surge on the south part of the south dome (Holdsworth, 1973a) and the work done on the ice margin at Generator Lake (Holdsworth, 1973b), we are in a position to reinterpret some of the observations made by Orvig (1953) and Ward (1953).

Orvig argued that the northeast side of the south dome, showing the highest shear stresses, should have the highest flow rates. Although this appears to be quite logical, it is found not to be the case if the velocity measurements

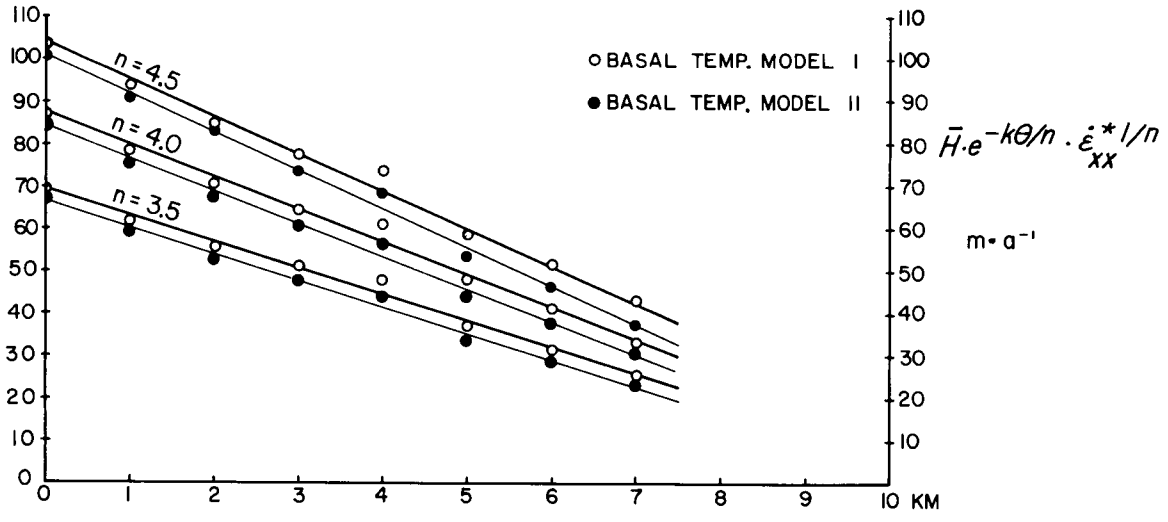

Figure 17. Plot of $\bar{H}e^{-k\theta/n}\dot{\varepsilon}_{xx}^{*1/n}$ versus distance along the flow line for various n values.

of Løken, Geiger and Langlais (1968) are correct. We have (Holdsworth, 1973a) tentatively identified these relatively high flow rates on the southwest side as due to the residual effects of a recent surge there. On the basis of observed marginal forms and moraine evidence, Orvig concluded that the whole ice cap (in the present study area) was migrating slowly northeast because of supposed asymmetry of the flow rates on opposite sides of the divide.

As the present data are unfavourable for the last supposition and because the known asymmetry in accumulation on either side of the divide (Løken and Andrews, 1966; Løken and Sagar, 1968; Holdsworth, unpublished data) is insufficient to account for a displaced divide (Weertman, 1973), we are led to believe that the latter phenomenon has been essentially caused by the surge. The actual reason, however, for the apparently steady (or advancing?) northeast margin and the apparently retreating southwest margin (apart from the surge lobe) must still be related to the mass balance.

Ward (1953), in commenting on Orvig's paper, speculated that if on the northeast side the margin was once flowing into proglacial lakes and the lake levels were subsequently lowered, the ice margin would advance and continue to do so for a long time. Although an ice advance following a rapid drawdown of water level is mechanically reasonable (Barnett and Holdsworth, 1974), there seems to be no new evidence to suggest that it has occurred or is still continuing on the northeast side. If the effect was the same as a "landslip" (surge?) (Ward, 1953), then one would expect to find on the northeast side an unusual surface profile (such as is found on the southwest side) and a divide displaced to the southwest.

Evidently Ward was seeking a mechanism that we now know as "surge triggering." Holdsworth (1973a) did not identify a definite "trigger mechanism" for the surge on the southwest side, although the implication was that through a steady buildup of superimposed ice sufficient area of the base would reach the pressure melting point, so that the outer ring of cold ice would be breached by the sliding of thick interior ice.

The geomorphological evidence (Løken and Andrews, 1966; Barnett and Holdsworth, 1974) is incomplete for the south lobe and might be interpreted in more than one way. In particular, a *detailed* subglacial topography and pre-surge lobe shapes for the south lobe are not yet known. [Radio echo sounding during April and May 1974 has provided new depth data (Jones and O'Neil, personal communication).] Therefore a tentative hypothesis for the "trigger mechanism" is now offered. When Generator Lake first emptied after a sufficient retreat of the ice margin, the lowering of the water level (removing a boundary constraint) could have led to the triggering of a surge, provided a sufficient percentage of the basal interior of the ice cap was at the pressure melting point. The surged ice would then have dammed up a lake once more. Obviously, this mechanism is cyclic; after long intervals of time the lake is catastrophically emptied only to fill up rapidly again as advancing (surge) ice blocks off the channel once more. (To produce the volume of water contained in the present lake approximately 20 years would be required.) If the duration of the surge cycle could be found, then we could estimate the number of past surges from the proposed chronology of Barnett and Holdsworth (1974).

Recent Information on the Surge Concept

Hooke (personal communication) has shown that the basal ice temperature gradient in two locations, about 1 km from the margin and 8 km to the northeast and 12 km to the east southeast of 000, is about 0.022 $^{\circ}C\ m^{-1}$ and 0.037 $^{\circ}C\ m^{-1}$, respectively. This opens the possibility of relating the three different surge areas (Løken, 1969) to the high (local) geothermal heat flow values.

ACKNOWLEDGEMENTS

The author would like to thank the 1970 and 1971 field personnel, especially C. Penton for his part in the 1970 survey. J. Paul Henderson advised on the use of the adjustment programs and J. Glynn wrote the additional programs necessary for reducing most of the data. Dr. S.J. Jones supplied ice thickness data and Dr. R. Le B. Hooke did the snow depth soundings in 1972 and 1973. Drs. W. Budd, R. Le B. Hooke, J. Weertman and I. Whillans constructively reviewed the manuscript.

REFERENCES

Barnett, D.M. and G. Holdsworth. 1974. "Origin Morphology and Chronology of Sublacustrine Moraines, Generator Lake, Baffin Island, N.W.T., Canada," *Canadian Journal of Earth Sciences,* Vol. II, No. 3, pp. 380-407.

Budd, W.F. 1969. "The Dynamics of Ice Masses." *ANARE Scientific Reports,* Series A (IV) Glaciology, Publication No. 108.

Henderson, J.P. "Report and Calculations for the Barnes Ice Cap Movement Survey, 1966." Unpublished ms.

Holdsworth, G. 1973a. "Evidence of a Surge on Barnes Ice Cap, Baffin Island," *Canadian Journal of Earth Sciences,* Vol. 10, No. 10, pp. 1565-1574.

Holdsworth, G. 1973b. "Ice Calving into the Proglacial Generator Lake, Baffin Island, N.W.T., Canada," *Journal of Glaciology,* Vol. 12, No. 65, pp. 235-250.

Hooke, R. Le B. Personal communication.

Hooke, R. Le B. 1973a. "Structure and Flow in the Margin of the Barnes Ice Cap, Baffin Island, N.W.T., Canada," *Journal of Glaciology,* Vol. 12, No. 66, pp. 423-438.

Hooke, R. Le B. 1973b. "Flow Near the Margin of the Barnes Ice Cap and the Development of Ice-Cored Moraines," *Geological Society of America,* Bulletin, 84, pp. 3929-3948.

Jenssen, D. and U. Radok. 1963. "Heat Conduction in Thinning Ice Sheets," *Journal of Glaciology,* Vol. 4, No. 34, pp. 387-397.

Jones, S.J. 1972. "Radio Depth-Sounding on Meighen and Barnes Ice Caps, Arctic Canada," *Scientific Series No. 25,* Department of the Environment, Inland Waters Directorate, Water Resources Branch, Ottawa, Ontario.

Jones, S.J. and R. O'Neil. Personal communication.

Løken, O.H. 1969. "Evidence of Surges on the Barnes Ice Cap, Baffin Island," *Canadian Journal of Earth Sciences,* Vol. 6, No. 4, Part 2, pp. 899-901.

Løken, O.H. and J.T. Andrews. 1966. "Glaciology and Chronology of Fluctuations of the Ice Margin at the South End of the Barnes Ice Cap, Baffin Island, N.W.T.," *Geographical Bulletin,* Vol. 8, No. 4, pp. 341-359.

Løken, O.H. and R.B. Sagar. 1968. "Mass Balance Observations on the Barnes Ice Cap, Baffin Island, Canada," Union de Géodésie et Géophysique Internationale, Association Internationale d'Hydrologie Scientifique, Assemblée générale de Berne, 1967, *Publication No. 79,* pp. 282-291.

Løken, O.H., A. Geiger and P. Langlais. 1968. "North Central Baffin Island Field Report 1967: Surface Movement and Strain Net Measurements—Barnes Ice Cap," Canada Department of Energy, Mines and Resources, Inland Waters Branch, *Report Series No. 2,* pp. 97-102.

Nye, J.F. 1957. "The Distribution of Stress and Velocity in Glaciers and Ice Sheets," *Proceedings of the Royal Society of London,* Series A, 239, pp. 113-133.

Nye, J.F. 1959. "A Method of Determining the Strain Rate Tensor at the Surface of a Glacier," *Journal of Glaciology,* Vol. 3, No. 25, pp. 409-419.

Orvig, S. 1953. "The Glaciological Studies of the Baffin Island Expedition, 1950, Part V: On the Variation of the Shear Stress on the Bed of an Ice Cap," *Journal of Glaciology,* Vol. 2, No. 14, pp. 242-247.

Peterson, A.E. "Program LEVELOB," *Technical Report No. 70-2,* Surveys and Mapping Branch, Department of Energy, Mines and Resources, Ottawa, Ontario. Unpublished ms.

Ward, W.H. 1953. Comments on Dr. Orvig's Paper, *Journal of Glaciology,* Vol. 2, No. 14, pp. 247-248.

Weertman, J. 1973. "Position of Ice Divides and Ice Centers on Ice Sheets," *Journal of Glaciology,* Vol. 12, No. 66, pp. 353-360.